Compositional and morphological analysis of high resolution remote sensing data over central peak of Tycho crater on the Moon: implications for understanding lunar interior

Prakash Chauhan[1,*], Prabhjot Kaur[1], Neeraj Srivastava[2], Satadru Bhattacharya[1], Ajai[1], A. S. Kiran Kumar[1] and J. N. Goswami[2]

[1]Space Applications Centre (ISRO), Jodhpur Tekra, Ahmedabad 380 015, India
[2]Physical Research Laboratory, Navarangpura, Ahmedabad 380 009, India

Tycho is a young impact crater of Copernican age (~ 110 Ma) in the southern highlands of the Moon. The crater has a well-developed central peak with an altitude of ~ 2 km. Central peaks of large lunar craters are ideal to study the deep-seated crustal material. In this study we report the results of an integrated morphological and compositional analysis for the central peak of the Tycho crater by using high-resolution data from Terrain Mapping Camera (TMC) and Moon Mineralogy Mapper (M3) on-board Chandrayaan-1 along with data from Narrow Angle Camera (NAC) of Lunar Reconnaissance Orbiter. Our analysis shows various morphological features associated with volcanism in the form of volcanic vents, domes, clasts, impact melt lava ponds showing distinct cooling cracks, and flow patterns on and around this central peak. Compositionally, M3 data suggest that the central peak is highly heterogeneous and dominated by high-Ca pyroxene-rich rocks. The base of the central peak is anorthositic in nature. These new morphological and mineralogical evidences suggest that the central peak of the Tycho crater has diverse morphology and mineralogical variability, suggesting multiphase modifications subsequent to the crater formation. The presence of diverse mafic lithologies on the central peak situated, in a predominantly anorthositic geological setting, suggests exposure of the subsurface pluton during the impact and thus provides insight into the composition of the lunar inner crust.

Keywords: Central peak, Chandrayaan-1, lunar interior, remote sensing, Tycho crater.

TYCHO, a prominent impact crater of ~ 100 km diameter is located in the southern highlands (43.4°S, 11.4°W) on the near side of the Moon and is considered as the classic example of a large impact carter. It is a young Copernican crater (~ 110 Ma) with well-developed bright ray patterns and intact crater morphology exhibiting a conspicuous central peak, sharply sculptured crater walls and rims with widespread ejecta blanket around its exterior[1]. Its central peak is believed to contain deep-seated material excavated during the impact and has been reported to have compositional assemblage of gabbroic nature with anorthositic rocks on its base[2–7]. The peak is also characterized by average titanium content > 1 wt%, showing the presence of mantle-derived mafic material of plutonic/volcanic origin[8]. Earlier studies on the Tycho crater indicated the possibility of volcanic activity on the central peak using photogeological studies of high resolution lunar orbiter photographs. Multiphase development of the central peak, involving late stage volcanism was inferred from Lunar Orbiter V images, which also revealed a possible lava pond on the central peak[9]. In a subsequent study, Tycho crater floor, rim and ejecta blanket using Lunar Orbiter V photographs were mapped and dated. Many lava flows and lava lakes on the crater floor, rim, terraced walls and a lava pond within the central peak were identified. Based on this it was concluded that the volcanism associated with Tycho crater may have been triggered by a large impact, which tapped a shallow subsurface source of magma[10]. Recent studies using very high resolution Lunar Reconnaissance Orbiter Narrow Angle Camera (LRO NAC) data suggest that the impact melt features around the Tycho are much younger than the ejecta blanket outside the crater[11]. The evidences for volcanic activity were also studied using morphology and morphometric analysis for 580 lunar craters (with diameter between 40 and 100 km) and only three craters, namely Lansberg (0.3°S, 26.6°W), Plinius (15.4°N, 23.7°E) situated in the mare region and Icarus (5.3°S, 173.2°W) situated in highland region, were considered to be plausibly modified or formed due to volcanic activity[12].

In this communication, we report results of a combined morphological and compositional analysis of new high resolution data over the central peak of the Tycho crater, to provide evidence for features associated with impact-induced volcanism/modifications using Terrain Mapping Camera (TMC) and Moon Mineralogy Mapper (M3) data from Chandrayaan-1 and NAC images of the LRO mission. Our study provides direct evidence of volcanism on this central peak, in the form of volcanic vents, clast/boulders, lava ponds showing prominent cooling cracks and lava channels with well-defined flow fronts at several locations. The compositional study using M3 data further shows the presence of heterogeneous mafic lithologies on the central peak, suggesting exposure of lunar inner crustal material.

Chandrayaan-1 TMC data with 5 m spatial resolution using three different stereoscopic views separated by ± 26° have been used to study the detailed morphological features. The TMC sensor operates in the panchromatic mode with a wide spectral range of 0.5–0.85 μm and covered a 20 km wide swath on the lunar surface. The three

*For correspondence. (e-mail: prakash@sac.isro.gov.in)

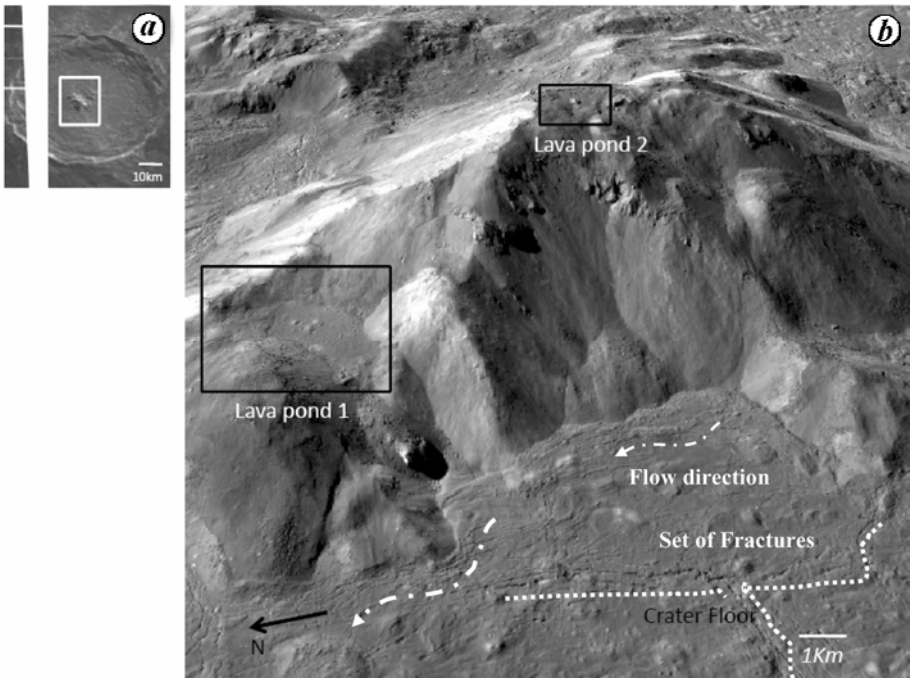

Figure 1. ***a***, Chandrayaan-1 TMC data mosaic of Tycho crater. ***b***, Three-dimensional image of Tycho central peak with vertical exaggeration factor of 5.0 showing two distinct lava ponds. Flow direction and pattern is marked with a thick dotted line. A set of fractures is marked with thin dotted lines.

stereo triplets of orbit number 2877 of TMC data were further used to generate digital elevation model (DEM) of the lunar surface at 25 m posting interval[13]. Additionally, LRO NAC datasets numbered M114031031LC, M111661378LE, M127008391LE and M104584909LE, obtained from the LRO website (http://wms.lroc.asu.edu), covering the central peak of Tycho crater and crater floor have been used for morphological analysis. Whereas TMC–DEM has provided a perspective view of the central peak (Figure 1), essential for the study of geologic settings and identification of various morphological features. LRO NAC data have enabled us to have a closer look at them from different phase angles, at a very high spatial resolution of ~0.5 m (Figures 2 and 3). Morphological parameters such as slope of the central rise have been generated and used for locating accumulation zones to understand the process of formation of lava ponds on the central rise (Figure 4).

For compositional analysis we have used hyperspectral data from the M3 sensor, guest instrument from NASA, on-board Chandrayaan-1[14,15]. M3 having the spectral range of 0.43–3.0 μm with 85 spectral bands acquired the spectral radiance data of the Moon surface in global mode, with 140 m/pixel spatial resolution from a 100 km orbit. For this study, the M3 Level-1b radiance data were converted into the apparent reflectance by normalizing the radiance values to incoming solar flux corresponding to spectral bands of the M3 data[16]. The apparent reflectance was converted using

$$\rho(\lambda) = \pi L(\lambda)/E_0(\lambda)\cos(\theta s), \quad (1)$$

where $\rho(\lambda)$ is the wavelength (λ)-dependent apparent reflectance, $L(\lambda)$ is the spectral radiance, $E_0(\lambda)$ is the incoming solar flux on the surface of the Moon and θs is the solar zenith angle. Spectral signatures of the central peak of the Tycho crater have been generated using reflectance data. Spectra have been limited up to 2.5 μm wavelength range to avoid thermal emission effects. Most of the sampled spectra were 3 × 3 pixel averages, whereas some were from 1 × 1 pixel due to smaller target size. These collected spectra were further used to assess the nature, distribution and association of the various mineralogical entities found on and around the Tycho crater.

The major lunar minerals consist of pyroxene, olivine, plagioclase and spinel with several other minor minerals like magnetite, ilmenite, etc. Spectroscopic remote sensing is one of the best tools to study planetary surface composition. The spectral properties of these minerals depend on their crystal structure and type of ions present in the crystallographic site of the minerals[17]. Olivine exhibits three overlapping absorption bands around 1.0 μm and lacks absorption band around 2.0 μm, Low-Ca pyroxenes exhibit two absorption bands between 0.90 and 0.93 μm, and 1.80 and 2.10 μm, and high-Ca clinopyroxene displays absorption bands between 0.91 and 1.06 μm and 1.97 and 2.35 μm (refs 17 and 18).

A variety of analytic tools have been developed to solve the mineralogical puzzles of the remote bodies using the positions of absorption bands present in reflectance spectra and their relative band areas[19–21], or by the deconvolution of near-infrared spectra into their component absorption bands[22]. For deriving mineralogical

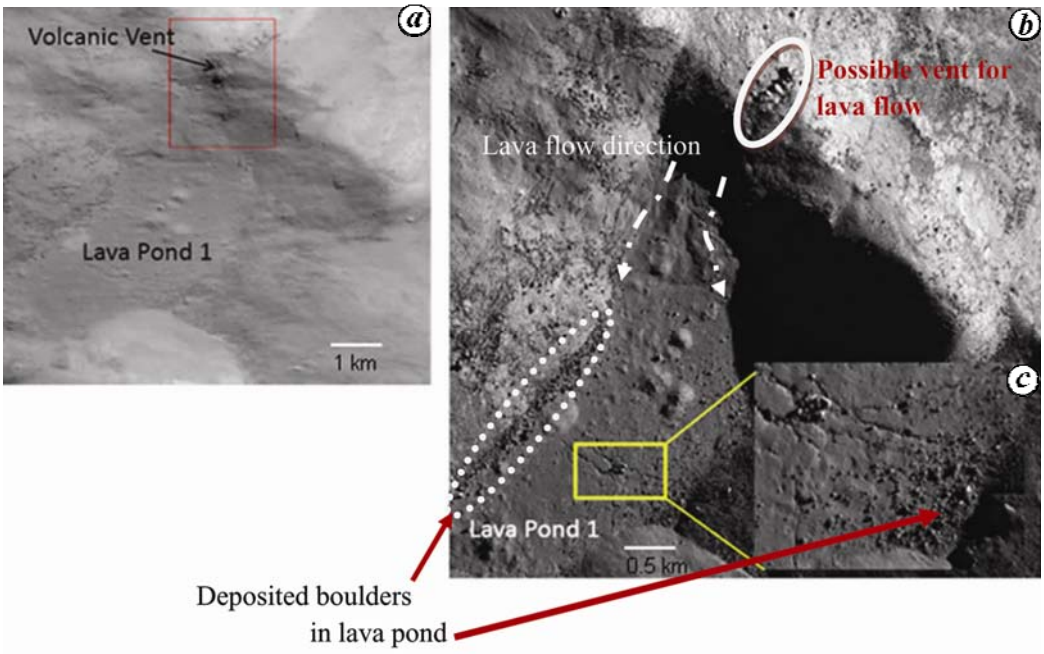

Figure 2. ***a***, High-resolution view of lava pond 1 using Chandrayaan-1 TMC data. ***b***, Very high-resolution view of the lava pond 1 from LROC NAC image. Possible vent for the lava flow is marked with a solid circle. Lava flow directions are marked with a thick dotted line; and clasts deposited at the base of the flank are marked with a dotted circle. ***c***, Close view of the lava pond showing fractures or fissures.

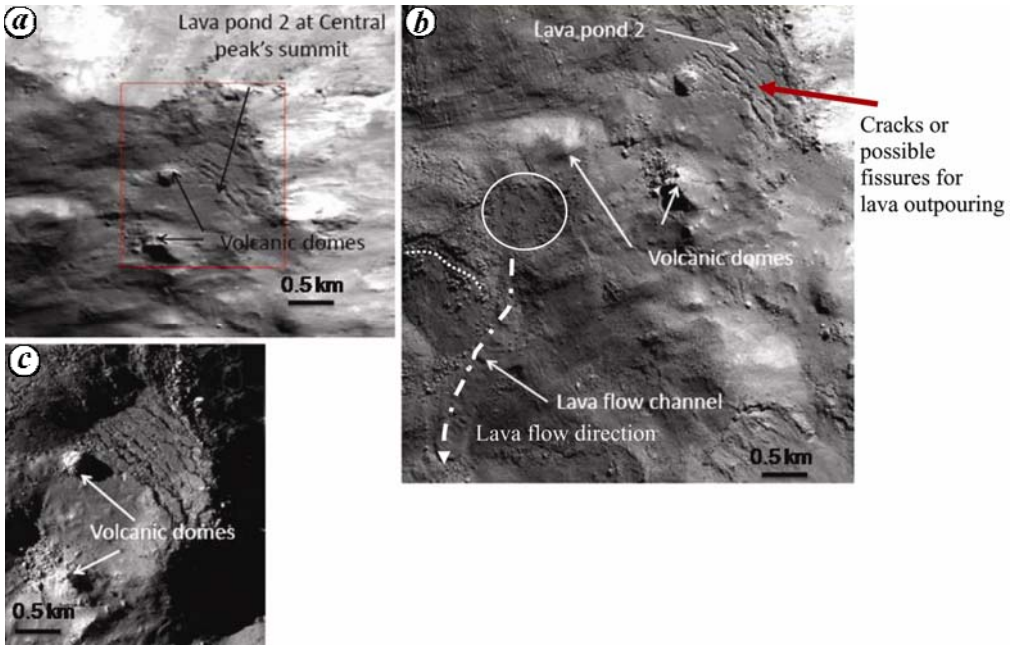

Figure 3. ***a***, High-resolution TMC image for lava pond 2 identified on the summit of the central peak clearly showing contractional cracks and volcanic domes. ***b***, LROC NAC image showing similar features in more detail along with lava channels on the slopes of the central peak. ***c***, LROC NAC image of same area showing domes with different sun angles.

information and characterization of the reflectance spectra, band analysis technique using scatter plot of central wavelengths for the first and second absorption features, developed by earlier workers is quite useful[21]. We performed a continuum removal technique on the reflectance spectra, to derive the central wavelengths around the first and second pyroxene absorption features called band I and band II respectively. Continuum removal has been performed to isolate specific absorption features and is accomplished by dividing out a straight line continuum tangent on either side of the absorption band. Band centres were calculated by fitting a third order polynomial to ~ 10–20 points on either side of a visually determined absorption centre or reflectance minimum.

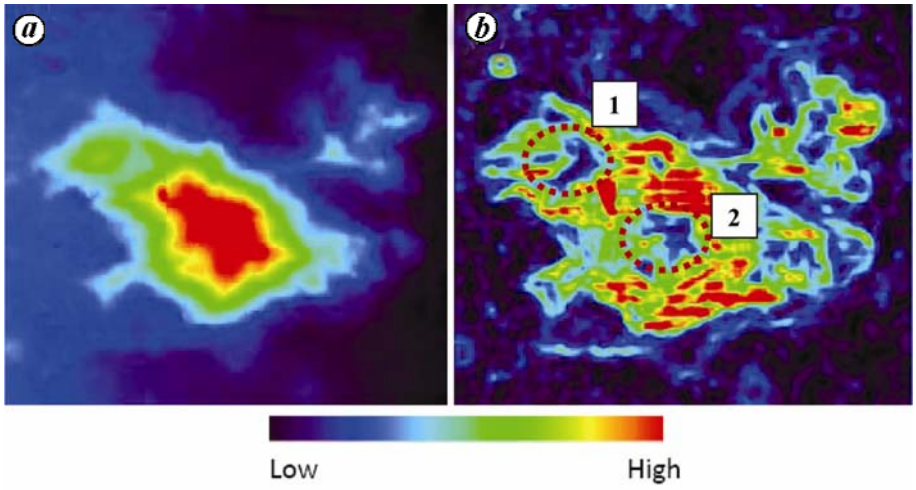

Figure 4. ***a***, Digital Elevation Model (DEM) of the central peak. ***b***, Slope map generated from TMC DEM. Locations (1) and (2) marked on slope map are depressions with gentle slope leading to accumulation for lava.

Figure 1 *a* shows a mosaic of TMC data strips covering the Tycho crater and Figure 1 *b* shows the three-dimensional view of the central peak, generated by draping the TMC panchromatic image over DEM. Using the DEM data a slope map for the central peak has been generated and is shown in Figure 4 *b*. Two accumulation zones having lesser slope have been identified using the slope map and are marked in Figure 4 *b*. Two lava ponds (marked 1 and 2 in Figure 1 *b*), with an aerial extent of ~ 1.4 and 0.5 sq. km respectively, have been identified and are associated with accumulation zones in the slope image. Lava pond 1 is located on the northwestern edge of the central peak, whereas lava pond 2 is located at the summit of the peak. Figure 2 *a* and *b* of lava pond 1, from TMC and LRO NAC data, clearly shows signatures of flow patterns associated with lava flow, clast/boulders and a slightly raised, inclined, volcanic vent of ~ 50 m diameter (Figure 2 *a*), surrounded by a high density of boulders. Some of the central peak areas are found to be covered with clast or boulders of varying size. The flow structures have been mapped and are marked in Figures 2 *b* and 3 *b*, with their possible flow direction indicated by arrows. The mapped flow structures follow the slope gradient of the flanks of the central peak. Possible vent for the lava flow which might have resulted into the formation of the lava pond 1 is also marked in Figure 2 *b*. Figure 2 *c*, the high resolution NAC image, shows the stratigraphic relationship between lava flow and overlaid clast, suggesting a time difference between the lava flow and deposition of the clasts embedded in the lava. It is evident from Figure 2 *b* that the lava flow must be older than the clasts/boulders which are embedded in the lava pond due to debris flow from the flank. The textural information suggests that at the time of deposition of the clasts, the lava must have been in a semi-solid state and not completely solidified leading to partial cementing of the clasts/boulders. Also some boulders can be easily seen (marked in Figure 2 *b*) deposited at the base of the flank, suggesting that slope instability resulted into the continuous debris flow from the flanks. The possible source of the lava channel is not clear; however, the presence of features like domes, fractures and a small circular depression (marked as thin dotted line in Figure 3 *b*) in the area points towards the possible sources of the lava channel. The other possible mode of formation of this channel is the flow of material from lava pond 2 first filling the circular depression followed by flow of the excessive material following the slope of the terrain. Figure 3 *a–c* of lava pond 2 at the summit of the central peak also shows peripheral contractional cracks associated with domes and clasts/boulders in close proximity. Figure 3 *b* shows a flow channel almost identical to the lava drainage channel having wrinkled/ropey appearance, suggesting the viscous nature of the lava compared to the lava flows in mare basins. The floor of the crater also exhibits hummocky flow pattern and well-developed fractures or contractional cracks (marked in Figure 1 *b*) developed as a result of cooling. These evidences suggest the volcanic nature of the morphological entities. The ropey appearance and contractional cracks as observed on the central peak and floor of the Tycho crater match well with the flow patterns associated with terrestrial lava.

Compositional variability of the Tycho crater is shown in a RGB combination generated using bands of the major absorption wavelengths (R = 1000, G = 1250 and B = 2000 nm) and draped over DEM, as shown in Figure 5 *a*. Figure 5 *b* and *c* shows a closer view of the central peak and the spectra collected from the various mineralogical entities respectively. In Figure 5 *a*, pyroxene-dominated lithologies are highlighted in green to yellow colours, and pink to blue shades represent anorthositic terrain. It is observed from Figure 5 *a* that the dominant lithology present on the central peak is pyroxene; however, the floor of the crater shows mixed lithology of anorthosite and pyroxene. The mineralogical diversity on the central peak has been captured in the

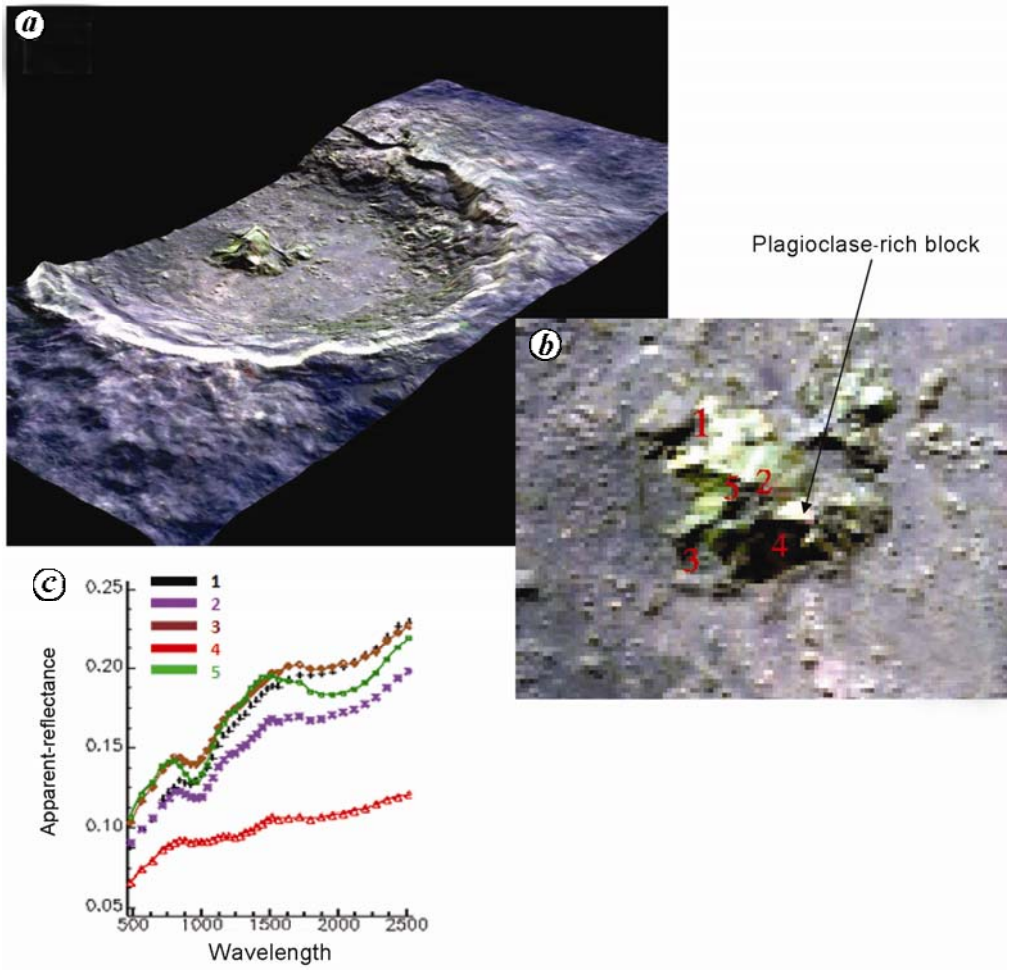

Figure 5. ***a***, Chandrayaan-1 M3 FCC generated using (1000, 1250 and 2000 nm bands) as RGB combination and draped over the radius image from M3 for a 3D perspective view of the Tycho crater. Greenish-yellow colour shows spatial distribution of mafic minerals. ***b***, Detailed view of central peak in FCC image and locations for spectra collected. ***c***, Spectral reflectance curves of the lava ponds 1 and 2 along with spectra of Tycho crater floor and plagioclase-rich blocks.

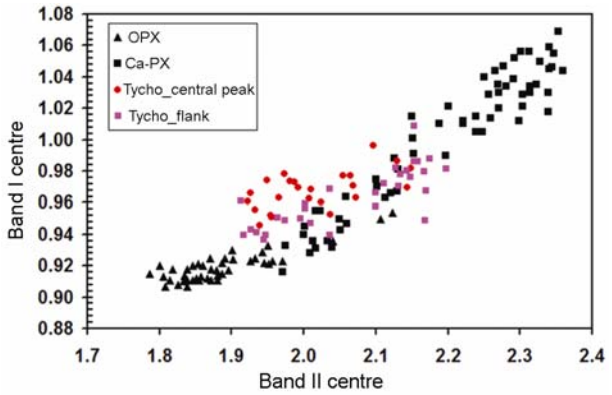

Figure 6. Two dimensional scatter plot of band centres of Pyroxene absorption features around 1000 nm (Band I) and 2000 nm (Band II). Band centre data from the flank area plots mostly within the pure pyroxene range whereas central peak band centres deviates from the regular trend.

spectra, collected at various locations, as shown in Figure 5 *b*. Spectra collected from the central peak region show prominent absorption at 1 and 2 μm corresponding to pyroxene (Figure 5 *c*). Spectrum 4 represents the plagioclase-rich flank, as it shows a prominent absorption feature around 1.3 μm. Similar results were also reported in a previous work using SELENE Multiband Imager (MI) data[7]. Apart from the 1.3 μm plagioclase feature, spectrum 4 also shows 1 and 2 μm absorption due to mixing with pyroxene. However, this information could not be captured by SELENE MI data due to lack of bands beyond 1.5 μm.

Band centres calculated as described earlier were used to determine the type of pyroxene present in the study area. Since for both types of pyroxene, the absorption features are different, the scatter plot of absorption at bands II and I is useful in determining the type of pyroxene[20,23]. Band II position is directly related to pyroxene composition, while band I is sensitive to the presence of relative composition and abundance of olivine and pyroxene component. A large number of spectra was collected from various part of the Tycho crater and a 2D scatter plot of band I and band II centres was generated, as shown in Figure 6. The band centre positions of spectra

from the central peak are shown as red dots, while pink squares represents spectra from the flanks. Black squares and triangles represent band centre data for synthetic ortho- and clinopyroxene[21]. The band centres for the Tycho crater falls in the sub-calcic-augitic (clinopyroxene) range when compared with the synthetic ortho- and clinopyroxene band–band plot[20,23,24]. The band centre data from the flank of the Tycho crater plot within the pure pyroxene range, whereas data from the central peak deviate much from the regular trend, showing the presence of an additional mineral phase(s). Based on the central wavelength of the collected spectra from the central peak and flank of the Tycho crater, it can be inferred that the central peak contains high-Ca pyroxene-bearing lithologies and these may be of plutonic origin, owing to the location of the Tycho crater far away from the basaltic mares. Presence of mafic lithology on the central peak of a lunar crater located in the highland area, also can be due to excavation of plutonic body during rebound or due to volcanic activity on the central peak at some stage. Considering the young age of the Tycho crater and its considerable distance from nearby mare basalts units, possibility of mafic ejecta cover from an adjacent younger impact event over the central peak is quite unlikely. Therefore, the possibility of exposure of pluton during the rebound assumes significance.

The volcanism associated with the Tycho crater and its central peak is not well established at present. This work clearly brings out the presence of morphological features like domes, fractures, lava ponds, lava channels, etc. on the central peak. The morphological analysis shows that the volcanic features are impact-induced and have been formed due to melting of the surface or subsurface lithologies. The mineralogical study suggests the presence of high-Ca pyroxene-bearing lithologies on the central peak. The presence of plagioclase-rich central peak suggests that mechanical processes involving rebound would have resulted in the formation of the anorthositic central peak, which appears to have got compositionally modified due to subsequent eruption of the subsurface plutonic body. These findings have important implications towards the understanding of the mechanism of formation and evolution of central peaks, in general, and late-stage volcanic activity on the Moon much beyond the impact of the Tycho crater, in particular.

1. Pohn, H. A., Geologic map of the Tycho quadrangle of the moon, I-713 (LAC 112), US Geological Survey, 1972, Washington DC, USA.
2. Hawke, B. R., Lucey, P. G. and Bell, J. F., Spectral reflectance studies of Tycho crater: preliminary results. *Lunar Planet. Sci. Conf.*, 1986, **XVII**, 999–1000.
3. Lucey, P. G. and Hawke, B. R., A remote mineralogic perspective on Gabbroic units in the lunar highlands. Proc. 19th Lunar Planetary Science Conference, Texas, USA, 1988, pp. 355–363.
4. Pieters, C. M., Compositional diversity and stratigraphy of the lunar crust derived from reflectance spectroscopy. In *Remote Geochemical Analysis: Elemental and Mineralogical Composition* (eds Pieters, C. M. and Englert, P.), Cambridge University Press, Houston, Texas, USA, 1983, pp. 309–336.
5. Tompkins, S. and Pieters, C. M., Mineralogy of lunar crust: results from Clementine. *Meteoritics Planet. Sci.*, 1999, **34**, 25–41.
6. Matsunaga, T. *et al.*, Discoveries on the lithology of lunar crater central peaks by SELENE Spectral Profiler. *Geophys. Res. Lett.*, 2008, **35**, L23201, doi: 10.1029/2008GL035868.
7. Ohtake, M. *et al.*, The global distribution of pure anorthosite on the moon. *Nature*, 2009, **461**, 236–240.
8. Srivastava, N., Titanium estimates of the central peaks of lunar craters: implications for sub-surface lithology of moon. *Adv. Space Res.*, 2008, **42**(2), 281–284.
9. Storm, R. G. and Fielder, G., Multiple eruptions associated with the lunar craters Tycho and Aristarchus. *Commun. Lunar Planet. Lab. Univ. Ariz.*, 1970, **8**, 150, 235.
10. Storm, R. G. and Fielder, G., Multiphase development of lunar crater Tycho. *Nature*, 1968, **217**, 611–615.
11. Hiesinger, H., Vander Bogert, C. H., Robinson, M. S., Klemm, K. and Reiss, D., New crater size frequency distribution measurements for Tycho crater based on Lunar Reconnaissance Orbiter camera analysis. Lunar Planetary Science Conference, XLI, 2010, Abstr. 2287.
12. Allen, C. C., Central peaks in lunar craters. *Moon*, 1975, **12**, 463–474.
13. Gopala Krishna, B., Amitabh, Singh, S., Srivastava, P. K. and Kiran Kumar, A. S., Digital elevation models of the lunar surface from Chandrayaan-1 Terrain Mapping Camera (TMC) imagery. Lunar Planetary Science Conference, XL, 2009, Abstr. 1694.
14. Goswami, J. N. and Annadurai, M., Chandrayaan-1: India's first planetary science mission to the moon. *Curr. Sci.*, 2009, **96**, 486–491.
15. Pieters, C. M. *et al.*, The Moon Mineralogy Mapper (M^3) on Chandrayaan-1. *Curr. Sci.*, 2009, **96**, 500–505.
16. Green, R. O., Pieters, C. M., Boardman, J., Lundeen, S. and Staid, M., The M3 Team, The Moon Mineralogy Mapper data set delivered to the Planetary Data System and calibration and validation status. *Lunar Planet. Sci.*, 2011, **42**, Abstr. 2089.
17. Burns, R. G., *Mineralogical Applications of Crystal Field Theory*, Cambridge University Press, New York, 1970, p. 224.
18. Burns, R. G., *Mineralogical Applications of Crystal Field Theory*, Cambridge University Press, Cambridge, UK, 1993, 2nd edn, p. 551.
19. Cloutis, E. A., Gaffey, M. J. and Reed, K. L., Calibrations of phase abundance, composition, and particle size distribution for olivine–orthopyroxene mixtures from reflectance spectra. *J. Geophys. Res.*, 1986, **91**, 11,641–11,653.
20. Cloutis, E. A. and Gaffey, M. J., Spectral compositional variations in the constituent minerals of mafic and ultra-mafic assemblages and remote sensing applications. *Earth, Moon, Planets*, 1991, **53**, 11–53.
21. Gaffey, M. J., Cloutis, E., Kelley, M. and Reed, K., Mineralogy of asteroids. In *Asteriods III* (eds Bottke, W. F. *et al.*), The University of Arizona Press, Arizona, USA, 2002, pp. 183–204.
22. Sunshine, J. M. and Pieters, C. M., Determining the composition of olivine from reflectance spectroscopy. *J. Geophys. Res.*, 1998, **103**, 13675–13688.
23. Adams, J. B., Visible and near-infrared diffuse reflectance spectra of pyroxenes as applied to remote sensing of solid objects in the solar system. *J. Geophys. Res.*, 1974, **79**, 4829–4836.
24. Klima, R. L., Dyar, M. D. and Pieters, C. M., Near-infrared spectra of clinopyroxenes: effects of calcium content and crystal structure, *Meteoritics Planet. Sci.*, 2011, **46**, 379–395.

ACKNOWLEDGEMENT. We thank the LROC NAC, Moon Mineralogy Mapper and SELENE MI teams for providing the data used in this work through public access web portals.

Received 13 February 2012; accepted 24 February 2012